# Infrared spectral responses of the Ocean Color Instrument (OCI) pre-assembly and integration

Jacob K. Hedelius[a], Kenneth J. Squire[a], James Q. Peterson[a], Branimir Blagojević[b], Ulrik B. Gliese[c], Eric T. Gorman[b], David K. Moser[a], Zakk Rhodes[a], Pedro Sevilla[a], and Gerhard Meister[d]

[a]Space Dynamics Laboratory, Utah State University, 416 E. Innovation Avenue, North Logan, UT 84341, USA
[b]NASA Code 592, Goddard Space Flight Center, Greenbelt, MD 20771, USA
[c]KBR Inc., 8120 Maple Lawn Blvd, Fulton, MD 20759, USA
[d]NASA Code 616, Goddard Space Flight Center, Greenbelt, MD 20771, USA

## ABSTRACT

Spectral characterizations were made of the Ocean Color Instrument (OCI) short-wave infrared (SWIR) Detection Subassembly (SDS) responses (940–2260 nm) prior to their integration. Using modulated output light from a Fourier transform spectrometer, the in-band relative spectral responses of the nine different configurations of SDSs were found along with out-of-band (OOB) sensitivity. From these spectral responses, the center wavelengths ($\lambda_0$), full widths at half of the maximum, full widths at 1% of the maximum, and OOB rejection ratios were determined. All spectral parameters are within requirements. There are 2–8 repeats of each configuration, and the $1\,\sigma$ spread among repeats is largest for the 1250 nm and 1615 nm high-gain configurations and is greater than 1 nm. The engineering requirement is for these values to be within ±4 nm and ±10 nm, respectively, of the nominal $\lambda_0$. There is also a $\lambda_0$ temperature dependence, which is expected. This temperature dependence is nearly a linear function of wavelength with a $9.5 \times 10^{-3}$ nm $K^{-1}$ relationship on average.

**Keywords:** PACE, OCI, Pre-Launch, SWIR, RSR, OOBRR, FWHM

## 1. INTRODUCTION

Observations from the Plankton, Aerosol, Cloud, ocean Ecosystem (PACE) Earth-observing satellite will provide insight into the Earth system by measuring light in bands of interest for observing the atmosphere, ocean color, and land. PACE is currently scheduled to launch no earlier than January 2024 into a sun synchronous polar orbit, with a 1300 local time equatorial crossing.[1] The Ocean Color Instrument (OCI) is the primary instrument on PACE and has a rotating telescope that will scan cross track in a west-to-east direction, with a nominal nadir ground sampling distance of 1 km and a swath width of 2,660 km.[1,2] From the telescope, light is directed to two grating spectrometers that will measure light from 340 to 890 nm at a 5 nm nominal spectral point spacing. Light is also directed to a third, short-wave infrared (SWIR) Detection Assembly (SDA) that will measure light in seven discrete bands of interest from 940 to 2260 nm. Two bands in the SDA have both high- and standard-gain configurations, for a total of nine different configurations. Goddard Space Flight Center (GSFC) built the telescope and grating spectrometers, and Utah State University Space Dynamics Laboratory (SDL) built the SDA. For a detailed technical description of OCI, see Ref. 3.

Measurements from the SDA bands are used in the retrievals of aerosol-related products and in deriving atmospheric corrections. For example, the 940 nm band, which is also used by the Aerosol Robotic Network (AERONET), is used in calculating total precipitable water vapor. The 1378 nm band, which is particularly sensitive to cirrus clouds and water vapor, may be used to correct for their effects. A list of the bands is in Table 1, along with band width requirements.[1,4] The full width at half of the maximum (FWHM) requirement

Send correspondence to J.K.H.
J.K.H.: E-mail: jacob-hedelius@sdl.usu.edu, Telephone: 1 435 713 3972

Table 1. OCI SWIR band requirements and characteristics. Listed purposes are examples only. SWIR bands may have multiple uses. n=total quantity or number of repeats, SG=standard-gain, HG=high-gain, Ocn=ocean, Atm=atmosphere

| | Band (nm) | FWHM (nm) | n | OOBRR ($\times 10^4$) | Other paired band(s) | Ocn or Atm | Example Purpose |
|---|---|---|---|---|---|---|---|
| A | $940 \pm 4$ | $45 \pm 4$ | 2 | 75 | E | A | Atmospheric water |
| B | $1038 \pm 2$ | $75 \pm 4$ | 4 | 75 | H, I | O | Water reflectance |
| C | $1250 \pm 4$ (SG) | $30 \pm 4$ | 2 | 75 | F | A | Aerosols |
| D | $1250 \pm 4$ (HG) | $30 \pm 4$ | 8 | 75 | G | O | Water reflectance |
| E | $1378 \pm 2$ | $15 \pm 2$ | 2 | 50 | A | A | Cirrus clouds |
| F | $1615 \pm 10$ (SG) | $75 \pm 10$ | 2 | 75 | C | A | Aerosols |
| G | $1615 \pm 10$ (HG) | $75 \pm 10$ | 8 | 75 | D | O | Water reflectance |
| H | $2130 \pm 5$ | $50 \pm 5$ | 2 | 75 | B | A | Ice vs. water clouds (w/2260) |
| I | $2260 \pm 10$ | $75 \pm 5$ | 2 | 75 | B | Both | Ice vs. water clouds (w/2130) |

constrains the spectral width of bands, and the full width at 1% of the maximum (FW1P) requirement is that it be less than two times the nominal FWHM. Bands were chosen to minimize transmission losses due to atmospheric absorption, while being located in spectral regions of interest to estimate geophysical parameters, such as cloud particle sizes, precipitable water vapor, and aerosol optical depth.[1,4] Bands were also chosen based on heritage measurements, such as the Moderate Resolution Imaging Spectroradiometer (MODIS) and Visible Infrared Imaging Radiometer Suite (VIIRS) to maintain continuity.

Some bands have detectors configured in both high-gain (HG) and standard-gain (SG) modes. To increase the signal-to-noise ratio (SNR), there are 2–8 repeats of each configuration. These are assembled into subunits called SWIR Detection Subassemblies (SDS). There are 16 SDSs each containing two physical detection channels, for a total of 32 discrete channels. Light is directed to each detector in the SDS units through dichroic filters, with reflected light going to the shorter wavelength channel. The 16 SDSs assembled together, along with relevant electronics and optical components, form the SDA.

Here we describe tests related to the spectral response characterization of the SDA conducted at SDL prior to delivery and integration of the SDA into OCI. We first describe the stages of assembly and tests conducted to characterize the spectral response in Sec. 2. Next, we discuss how measurements conducted were analyzed, so they could be compared against mission design requirements (Sec. 3). Results are described across different stages of assembly in Sec. 4. Section 5 contains concluding remarks.

## 2. OCI AND COMPONENT TESTS

There were three stages at which the spectral responses of the flight OCI SWIR detectors could be tested. These include 1) tests on individual SDS units, 2) tests at SDL on the assembled SDA, and 3) tests at GSFC after integration of the SDA into OCI. Engineering Test Unit (ETU) measurements at GSFC were described previously in Refs. 5 and 6, and should not be confused with the tests described here on the flight unit. Results herein are from the SDS and SDA levels of assembly and thus do not include contributions from the OCI telescope. Spectral measurements at the full OCI level of assembly are scheduled at GSFC at the nominal temperature.

During calibration testing, a variety of measurements are taken to characterize the system performance. These include dark responses, absolute responses, repeatability, saturation recovery, frequency responses, linearity, in-band relative spectral responses (RSR), and out-of-band (OOB) responses. This paper focuses on the last two for flight unit tests conducted at SDL. Linearity characterization results are discussed in Ref. 7. Tests were conducted from late 2020 through early 2021, and the SDA was delivered to GSFC in July 2021. All tests were conducted under flight-like thermal vacuum conditions. SDS tests were conducted at their nominal operational temperature of −65°C, and SDA tests were conducted at both hot qualification temperature (−55°C) and cold qualification temperature (−75°C).

Spectral parameters of interest are described in Ref. 5, which we briefly repeat here. First, lower and upper wavelengths (we denote as $\lambda_{-1}$ and $\lambda_1$) for the FWHM are empirically determined, from which the center wavelength is found using:

$$\lambda_0 = \frac{\lambda_1 + \lambda_{-1}}{2}\,, \tag{1}$$

and

$$\mathrm{FWHM} = \lambda_1 - \lambda_{-1}\,. \tag{2}$$

The full width at 1% of the maximum (FW1P) limits are found in the same manner as the FWHM and are denoted $\lambda_{-2}$ and $\lambda_2$. The OOB rejection ratio (OOBRR), also referred to as the integrated OOB response ratio, in theory is determined with

$$\mathrm{OOBRR} = \frac{\int_0^{\lambda_{-2}} R_S\left(\lambda\right) d\lambda + \int_{\lambda_2}^{\infty} R_S\left(\lambda\right) d\lambda}{\int_{\lambda_{-2}}^{\lambda_2} R_S\left(\lambda\right) d\lambda}\,, \tag{3}$$

where $R_S$ is the spectral response weighted by a reference solar spectrum.[8–10] Here, the $\lambda_{-2}$ and $\lambda_2$ limits are the maximum FW1P specified by the requirements. In practice we cannot integrate over all wavelengths from zero to infinity due to limits in the light source and modulated input signal, so we integrated from 800 nm on the low end to 2500 nm on the high end (2800 nm for bands 1615, 2130, and 2260 nm). We emphasize that the numerator is of the actual detector OOB response and not just of the noise. Though unspecified in the system requirements, we also calculate the average spectral response across the FWHM ($\mathrm{ASR}_{\mathrm{FWHM}}$).

A sketch of the measurement setup is shown in Fig. 1, and this technique has also been described previously.[11–13] The Bruker Invenio step-scan Fourier transform spectrometer (FTS) has an internal lamp with a broadband visible-infrared (vis-IR) source. This light is directed through the interferometer and out one of the exit ports. For in-band SDA RSR characterizations, light was directed into a 12-inch integrating sphere. Attached to the sphere was a bundle of 16 output fibers to the SDA (or a single fiber for SDS testing), a reference detector for characterizing the relative spectral output (RSO) of the system, and an LED connected to the FTS that sent in a pulsed signal whenever the internal FTS HeNe metrology laser hit a crossing, and the interferometer was held at a new step. The LED was changed as needed to one where the wavelength was matched with the response of one of the detectors being tested. Due to size constraints, different chambers were used for SDS testing compared to SDA testing. SDS testing also required the use of an external Data Acquisition (DAQ) system, whereas the SDA had its own electronics, which were used when it was tested.

OOB characterization could be accomplished using the same setup with longer or multiple collects. However, since the SNR only improves with nominally $\sqrt{n}$, collects would need to be orders of magnitude longer, which would be temporally prohibitive. Further, temporal drift or 1/f noise limits the advantage of longer averaging

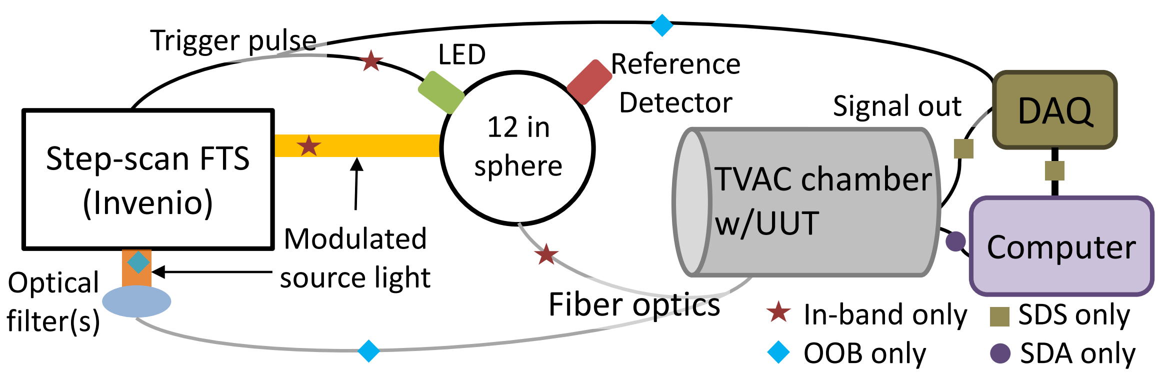


Figure 1. Sketch of the spectral response measurement setups. Some paths are only used for some of the characterizations, indicated by the red stars, blue diamonds, tan squares, or purple circle. For in-band characterizations, FTS source light is mixed with an LED pulse signal before going through the fiber optic cable (or 16 cables for SDA testing) to the detectors. The SDA has its own electronics, so the DAQ used for SDS testing was not needed. For OOB tests, only one of the SDS channels is tested at a time, which leaves a DAQ channel open for the trigger pulse to be sent to it directly. UUT=Unit Under Test

times. Instead, the FTS output was directed through different combinations of filters. For each of the nine different detector types, a minimum of three different filter combinations with known transmittance were used for separate collects, including one using neutral density filters, one for passing shorter wavelengths ("blue"), and one for passing longer wavelengths ("red"). OOB characterization requires a minimum of 32 (detectors) $\times 3$ (filters) $= 96$ collects and was only performed at the SDS assembly level. Acquisition takes approximately 10 minutes per double-sided interferogram. A total of 3553 steps are acquired, which is equivalent to a maximum optical path difference of 0.056 cm or an optical resolution of 16 cm$^{-1}$ (about 4 nm at 1600 nm).

## 3. ANALYSIS METHODS

We create interferograms from the step-scan measurements. We average 0.08 s of data per step, and discard the remaining 0.045 s to not include the influence of the pulse signals. Samples up to approximately 0.05 cm maximum optical path difference (MOPD) are included, with the actual MOPD used dependent on band. Zero filling is applied before the fast Fourier transform (FFT) to decrease the spectral point spacing distance. A Kaiser-Bessel apodization is also applied to the interferogram to reduce ringing in the spectrum. After the FFT, the spectrum is corrected to account for the RSO of the system, including any optical filters. For in-band spectra, the RSR is obtained by normalizing, so the peak in-band response is equal to one. OOB spectra are normalized relative to each other before being merged together. Typically, merged spectra are created with the

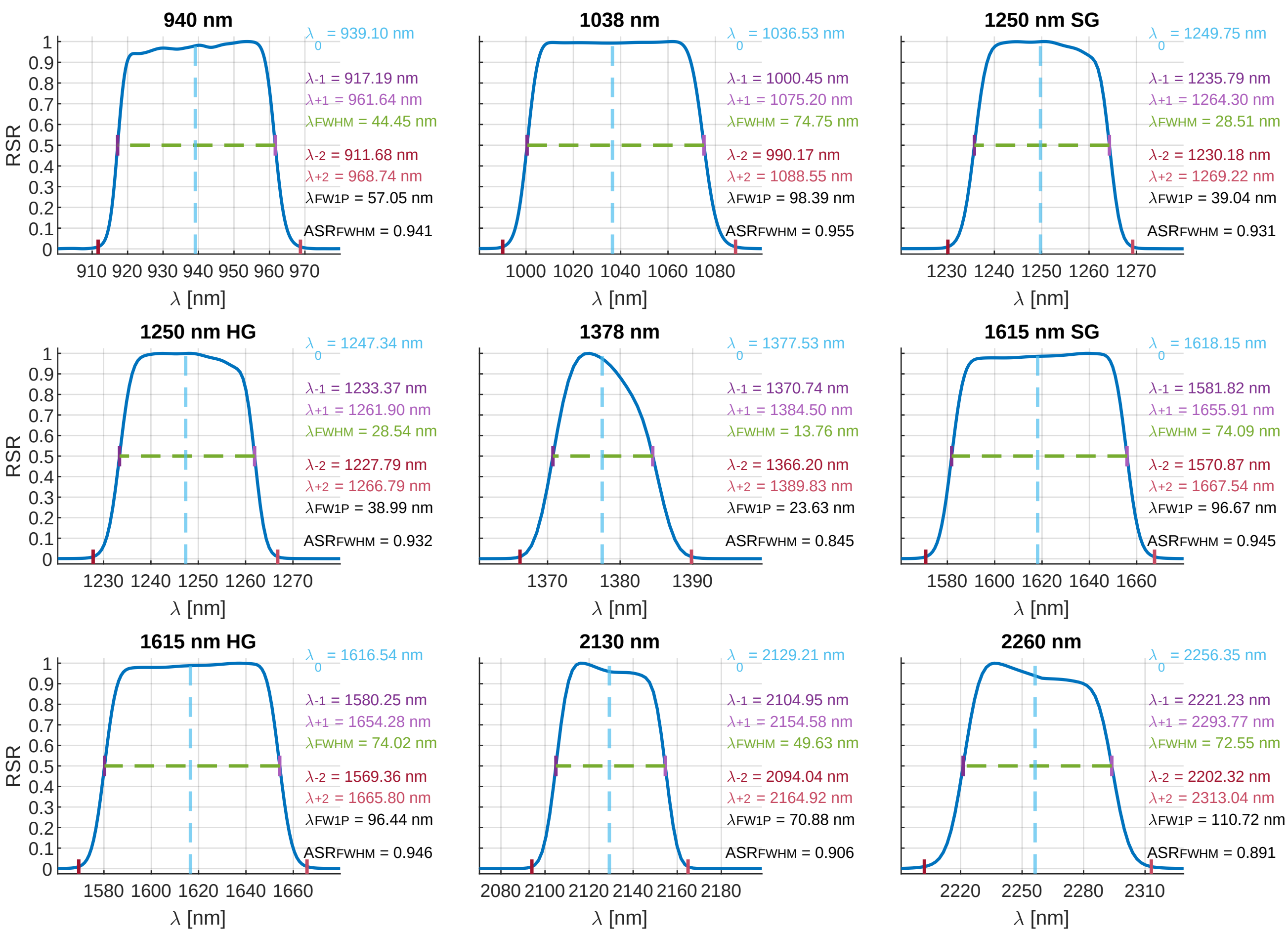


Figure 2. Example RSRs for each of the different types of detectors. Responses were acquired at the flight unit SDA level during cold qualification testing.

in-band spectra used for the FW1P region, with the blue-pass spectra for shorter wavelengths, and the red-pass spectra for longer wavelengths.

The spectral points $\lambda_{-2}$, $\lambda_{-1}$, $\lambda_1$, and $\lambda_2$ are found as the first points to meet 1% or 50% of the maximum signal going outwards from the nominal $\lambda_0$. OOB spectra are multiplied by the 2000 ASTM (American Society for Testing and Materials) Standard Extraterrestrial Spectrum[8–10] before the OOBRR is calculated.

# 4. RESULTS

## 4.1 Individual Detector Results

Relative spectral responses are measured for each of the different types of detection channels. The RSRs are also known as the Spectral Response Functions (SRFs) for some programs. Representative RSRs for each channel type, including band location and gain, are shown in Fig. 2. All RSR spectral parameters ($\lambda_0$, FWHM, and FW1P) are in compliance with requirements. These responses were acquired with an FTS, and interferograms were apodized using a Kaiser-Bessel function, which is based on a zeroth order Bessel function of the first kind. This function reduces the side lobes of a sinc function by about a factor of 100, but increases the FWHM of the sinc function by approximately 77%. These effects slightly smooth the RSR transitions on both edges, decreasing the $\mathrm{ASR_{FWHM}}$ and increasing the FW1P. This is on order of a 1% decrease in $\mathrm{ASR_{FWHM}}$ and a 1 nm increase in the FW1P, which is negligible compared to the requirements margin. We see the spectral response is not symmetric about $\lambda_0$, with the response often sloping with wavelength.

Three different RSR tests were conducted, including one at nominal operation temperature during SDS testing and both hot and cold qualification temperatures during SDA testing. Figure 3a shows the $\lambda_0$ for all of these tests and for all channels. Note the offset added in the x-direction, so points do not overlap. This plot reveals clustering for the 1250 nm and 1615 nm bands, likely from groups having optics that are more similarly matched. The differences in temperature also allow us to examine effects of temperature on spectral responses (Fig. 3b). Because thin film narrow bandpasses are incorporated into the SDS units, a temperature dependence of $\lambda_0$ is expected.[14] We find that, on average, hot qualification (HQ, $-55$°C) $\lambda_0$ values are $0.19\pm0.05$ nm larger than values at cold qualification temperatures (CQ, $-75$°C) for an average rate of $9.5\times10^{-3}$ nm K$^{-1}$. However, this dependence on temperature is different for the different bands and increases nearly linearly with wavelength

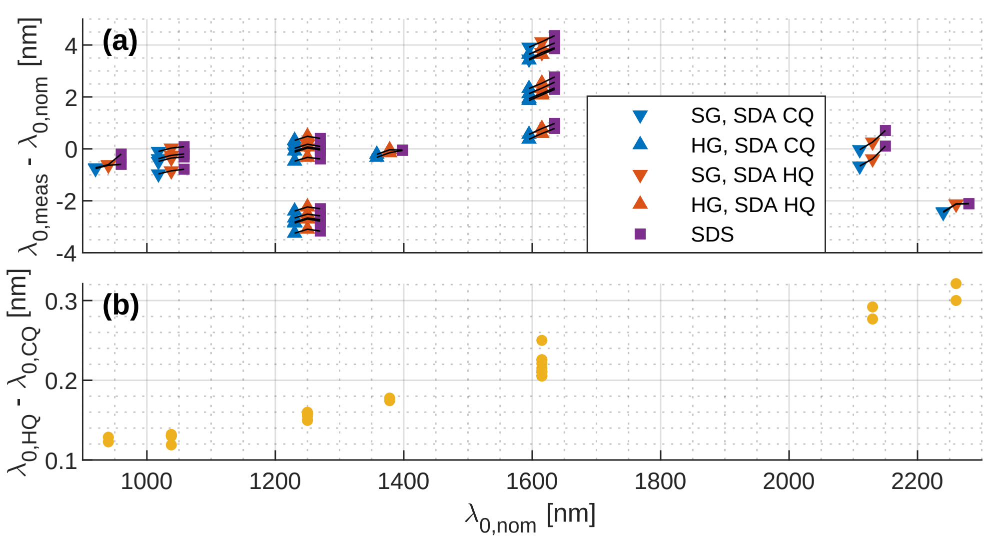


Figure 3. (a) Center wavelengths ($\lambda_0$) measured under different test conditions. Points are distinguished by detector gains (SG=standard-gain, HG=high-gain), temperatures (CQ=cold qualification, HQ=hot qualification), and assembly level (SDS, SDA). Note that the CQ and SDS measurements have been offset to the left and right, respectively, from nominal $\lambda_0$ for clarity. Black lines are guides for the same physical unit under different tests. (b) The difference between $\lambda_0$ measured at HQ and CQ as a function of the nominal $\lambda_0$. The difference is a function of wavelength.

Table 2. Sensitivity of the OCI SWIR channels $\lambda_0$ to different temperatures.

| Band (nm) | $\Delta\lambda_0 \cdot \Delta T^{-1}$ [nm $K^{-1}$] | Band (nm) | $\Delta\lambda_0 \cdot \Delta T^{-1}$ [nm $K^{-1}$] | Band (nm) | $\Delta\lambda_0 \cdot \Delta T^{-1}$ [nm $K^{-1}$] |
|---|---|---|---|---|---|
| 940 | $0.126 \pm 0.004$ | 1250 (HG) | $0.128 \pm 0.006$ | 1615 (HG) | $0.230 \pm 0.028$ |
| 1038 | $0.156 \pm 0.004$ | 1378 | $0.176 \pm 0.002$ | 2130 | $0.284 \pm 0.011$ |
| 1250 (SG) | $0.160 \pm 0.001$ | 1615 (SG) | $0.215 \pm 0.008$ | 2260 | $0.311 \pm 0.015$ |

(Table 2). Despite the SDS measurements being taken at the nominal temperature between HQ and CQ, $\lambda_0$ values are not always in between. This could be due to differences in measurement setups, including different optics.

### 4.2 Averaged Spectra

Multiple detection channels of the same band and gain provide redundancy and increase the total SNR for that wavelength band. Unweighted averages of the spectra acquired during SDS-level testing were also found along with their standard deviations. These spectra are shown in Fig. 4, separated by high-gain and standard-gain bands. Channels with $\lambda_0 > 1500$ nm use Leonardo HgCdTe detectors, where the quantum efficiency is known to decrease significantly below 1400 nm. This is due to a GaAs layer in the detector. This decrease has been added in during the processing of the OOB regions to better constrain the upper-bound of the measurements as shown. OOB sensitivity in regions below approximately 900 nm is expected to be reduced further when integrated into OCI due to the dichroics, which will split shorter wavelengths off to the grating spectrometers.

From the averaged spectra, we found the $\lambda_0$, FWHM, FW1P, and OOBRR values listed in Table 3. The means and standard deviations of individually determined values from Sec. 4.1 are also listed in Table 3. There is not a significant difference between determining the average of the spectral parameters versus averaging spectra and then computing the parameters.

## 5. CONCLUSION

The spectral responses of the SDSs, encompassing 32 channels, for the PACE OCI SDA are characterized for both their in-band and out-of-band responses. Tests were conducted at different stages of assembly and under

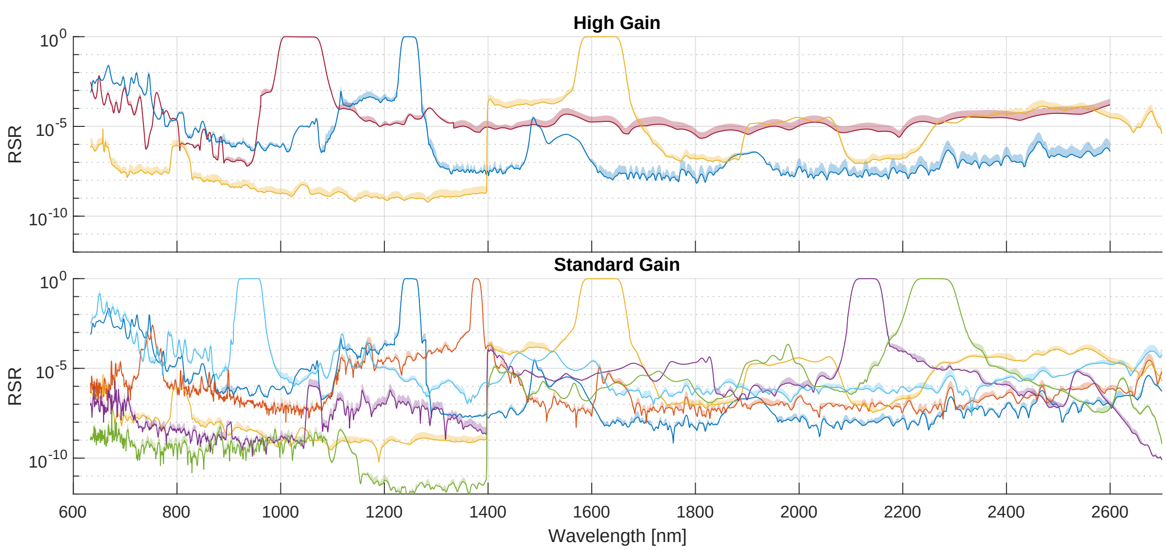


Figure 4. Averaged RSR and OOB merged spectra for each band and gain. Shaded regions represent $+1\sigma$ across repeats of a given configuration.

Table 3. OCI SWIR band averaged measured characteristics. The first columns of values are the means and standard deviations for the individual SDS characterizations. The second columns are values determined after first averaging spectra. Values are rounded to 1 decimal so standard deviations less than 0.05 are listed as 0.0.

| Band (nm) | $\lambda_0$ (nm) | | FWHM (nm) | | FW1P (nm) | | OOBRR ($\times 10^4$) | |
|---|---|---|---|---|---|---|---|---|
| 940 | $939.6 \pm 0.3$ | 939.6 | $44.5 \pm 0.0$ | 44.5 | $57.2 \pm 0.1$ | 57.2 | $1.6 \pm 1.9$ | 2.4 |
| 1038 | $1037.7 \pm 0.4$ | 1037.7 | $74.5 \pm 0.0$ | 74.5 | $98.3 \pm 0.1$ | 98.1 | $1.5 \pm 0.5$ | 1.5 |
| 1250 (SG) | $1250.0 \pm 0.1$ | 1250.0 | $28.7 \pm 0.2$ | 28.7 | $39.3 \pm 0.2$ | 39.2 | $6.2 \pm 0.6$ | 6.2 |
| 1250 (HG) | $1248.3 \pm 1.4$ | 1248.2 | $28.7 \pm 0.1$ | 28.7 | $39.4 \pm 0.1$ | 40.8 | $13.0 \pm 8.6$ | 13.0 |
| 1378 | $1377.9 \pm 0.0$ | 1378.0 | $14.2 \pm 0.0$ | 14.2 | $23.7 \pm 0.0$ | 23.6 | $30.4 \pm 2.5$ | 25.2 |
| 1615 (SG) | $1619.1 \pm 0.3$ | 1619.1 | $74.1 \pm 0.1$ | 74.1 | $96.3 \pm 0.0$ | 96.4 | $3.3 \pm 1.4$ | 3.3 |
| 1615 (HG) | $1617.5 \pm 1.2$ | 1617.5 | $74.0 \pm 0.0$ | 74.0 | $96.3 \pm 0.1$ | 96.7 | $4.8 \pm 3.5$ | 4.8 |
| 2130 | $2130.4 \pm 0.4$ | 2130.4 | $49.6 \pm 0.0$ | 49.6 | $70.9 \pm 0.0$ | 70.9 | $4.5 \pm 0.6$ | 4.5 |
| 2260 | $2257.9 \pm 0.0$ | 2257.9 | $72.8 \pm 0.1$ | 72.8 | $110.0 \pm 0.1$ | 110.0 | $5.1 \pm 1.3$ | 5.1 |

different temperatures. In-band responses are summarized by the center wavelengths ($\lambda_0$), FWHM, and FW1P. All in-band metrics meet the OCI system requirements. OOBRRs, or ratios between out-of-band responses to in-band responses for a typical solar spectrum, are also all within specifications.

The difference in center wavelengths between the standard-gain and high-gain bands at 1250 nm and 1615 nm is more than 1 nm (Table 3). In hindsight, there should have been a specification to require better agreement between the center wavelengths of the standard-gain and the high-gain bands, because some PACE science algorithms are planning to combine the data from both gains assuming both have the same spectral response. Similar missions in the future may consider adopting requirements for the range of center wavelengths among equivalent bands. Because this was not a requirement for this system, optics were not selected with this consideration. In addition to the variation in ($\lambda_0$) among similar physical channels within a single test, there are also systematic differences in ($\lambda_0$) for the same channels at different temperatures (Fig. 3). However, the dependence with temperature is to be expected due to the physical nature of the thin film optical filters used in the SDS units.

Note that the RSRs measured at SDA level are different from the OCI system-level RSRs. Differences include optical components of the telescope and components that direct light of wavelengths below approximately 900 nm to the grating spectrometers. The additional system-level components can affect the spectral responses. The in-band RSR parameters presented here should not be significantly affected by this difference, but it is important for below 900 nm OOB RSR.

## 6. AUTHOR CONTRIBUTIONS

JKH performed the formal analysis, created the visualizations and wrote the initial draft. JKH, KJS, JQP and GM reviewed and edited the paper. PS created the software used for data acquisition. KJS and DKM collected data used in analysis. ZR designed the SDA electronics. UBG was involved in SDA optical design, and BB was involved in SDA optical filter design. GM and ETG secured funding and provided project administration.


## ACKNOWLEDGMENTS

We thank the following for their contributions to this work: Paul Fluckiger for assembling the SDA, James A. Champagne for leading overall SDA optical design, Gabriel Loftus for leading SDA project management at the Space Dynamics Laboratory and Hannah Brailsford for technical review and editing.

We acknowledge contract funding through the NASA GSFC PACE program.


## REFERENCES


[1] Werdell, P. J., Behrenfeld, M. J., Bontempi, P. S., Boss, E., Cairns, B., Davis, G. T., Franz, B. A., Gliese, U. B., Gorman, E. T., Hasekamp, O., Knobelspiesse, K. D., Mannino, A., Martins, J. V., McClain, C. R., Meister, G., and Remer, L. A., "The Plankton, Aerosol, Cloud, Ocean Ecosystem Mission: Status, Science, Advances," *Bulletin of the American Meteorological Society* **100**, 1775–1794 (9 2019).

[2] Remer, L. A., Davis, A. B., Mattoo, S., Levy, R. C., Kalashnikova, O. V., Coddington, O., Chowdhary, J., Knobelspiesse, K., Xu, X., Ahmad, Z., Boss, E., Cairns, B., Dierssen, H. M., Diner, D. J., Franz, B., Frouin, R., Gao, B.-C., Ibrahim, A., Martins, J. V., Omar, A. H., Torres, O., Xu, F., and Zhai, P.-W., "Retrieving Aerosol Characteristics From the PACE Mission, Part 1: Ocean Color Instrument," *Frontiers in Earth Science* **7**, 1–20 (7 2019).

[3] Gorman, E., Kubalak, D. A., Deepak, P., Dress, A., Mott, D. B., Meister, G., and Werdell, J., "The NASA Plankton, Aerosol, Cloud, ocean Ecosystem (PACE) mission: an emerging era of global, hyperspectral Earth system remote sensing," in [*Sensors, Systems, and Next-Generation Satellites XXIII*], Neeck, S. P., Kimura, T., and Martimort, P., eds., **11151**, 15, SPIE (10 2019).

[4] Ahmad, Z., Arnone, R., Behrenfeld, M. J., Cairns, B., Cetinić, I., Eplee, R. E., Haffner, D., Ibrahim, A., Mannino, A., McKinna, L. I. W., Meister, G., Neeley, A., Pahlevan, N., Patt, F. S., Robinson, W., Signorini, S. R., Vandermeulen, R., and Westberry, T., "PACE Technical Report Series , Volume 7 Ocean Color Instrument (OCI) Concept Design Studies," Tech. Rep. TM–2018-219027, Goddard Space Flight Center, Greenbelt, Maryland (2018).

[5] Kitchen-McKinley, S., McIntire, J., Choi, H., and Meister, G., "PACE OCI Pre-launch ETU spectral characterization and performance," in [*Earth Observing Systems XXVI*], Butler, J. J., Xiong, X. J., and Gu, X., eds., 7, SPIE (8 2021).

[6] Meister, G., Knuble, J. J., Chemerys, L. H., Choi, H., Collins, N. R., Eplee, R. E., Gliese, U., Gorman, E. T., Jepsen, K., Kitchen-McKinley, S., Lee, S., Mcintire, J. W., Patt, F. S., Tse, B. C., Waluschka, E., and Werdell, P. J., "Test Results From the Prelaunch Characterization Campaign of the Engineering Test Unit of the Ocean Color Instrument of NASA's Plankton, Aerosol, Cloud and Ocean Ecosystem (PACE) Mission," *Frontiers in Remote Sensing* **3**, 1–15 (6 2022).

[7] Squire, K. J., Hedelius, J. K., Peterson, J. Q., Gorman, E. T., and Meister, G., "PACE OCI short-wave infrared detection assembly frequency-dependent linearity characterization and uncertainty analysis," in [*Earth Observing Systems XXVII*], SPIE (8 2022).

[8] NREL, "2000 ASTM Standard Extraterrestrial Spectrum Reference E-490-00," (2000).

[9] Myers, D. R., Emery, K., and Gueymard, C., "Revising and Validating Spectral Irradiance Reference Standards for Photovoltaic Performance Evaluation," *Journal of Solar Energy Engineering* **126**, 567–574 (2 2004).

[10] American Society for Testing and Materials, "Standard Solar Constant and Zero Air Mass Solar Spectral Irradiance Tables," Tech. Rep. Reapproved 2006, ASTM International, West Conshohocken, PA, USA (2006).

[11] Hansen, S., Peterson, J., Esplin, R., and Tansock, J., "Component level prediction versus system level measurement of SABER relative spectral response," *International Journal of Remote Sensing* **24**, 389–402 (1 2003).

[12] Peterson, J. Q., Hansen, S., and Thurgood, A., "SDL Experiences with Interferometric Testing of Sensor Spectral Characteristics," in [*19th Annual Conference on Characterization and Radiometric Calibration for Remote Sensing*], 1000–1021 (2010).

[13] Yoon, H. W. and Kacker, R. N., "Guidelines for Radiometric Calibration of Electro-Optical Instruments for Remote Sensing," Tech. Rep. April, National Institute of Standards and Technology, Gaithersburg, MD (5 2015).

[14] Stolberg-Rohr, T. and Hawkins, G. J., "Spectral design of temperature-invariant narrow bandpass filters for the mid-infrared," *Optics Express* **23**, 580 (1 2015).